Transportation Research Part C 19 (2011) 975–984

Contents lists available at ScienceDirect

Transportation Research Part C

journal homepage: www.elsevier.com/locate/trc

Railway wheel-flat detection and measurement by ultrasound ☆

J. Brizuela *, C. Fritsch, A. Ibáñez

Consejo Superior de Investigaciones Científicas (CSIC), La Poveda (Arganda del Rey), 28500 Madrid, Spain

ARTICLE INFO

Article history:
Received 17 November 2010
Received in revised form 18 April 2011
Accepted 20 April 2011

Keywords:
Wheel-flat detection
Rolling surface
Rayleigh waves
Railway NDE

ABSTRACT

This work presents an innovative ultrasound technique designed to detect and quantify flats formed in the rolling surface of railway wheels. Differently from other approaches, ultrasonic pulses (Rayleigh waves) are sent over a measuring rail. The variations in the round-trip time of flight (RTOF) of the ultrasound pulse to the rail-wheel contact point allow detecting and quantifying the wheel-flats. In spite of the wear state of the irregularity, the method provides the loss of material and the length of the flat originally formed by abrasion. A theoretical background supports the technique which offers many advantages for railway maintenance. Simulations and experimental results match the expected ones.

1. Introduction

During the braking process in railway transport, sometimes the wheel locks and slides along the rail. The reason for this may be a defective, frozen or incorrectly tuned brake, as well as a low wheel-rail adhesion caused by environmental conditions (rain, snow, leaves, etc.). The abrasive effect of skidding causes a high wear on the rolling surface (a flat), with lengths ranging typically from 20 to over 100 mm.

The rise in temperature caused by abrasion, followed by a fast cooling, may lead to the formation of brittle martensite beneath the flat. This is in the origin of further flaws like cracks and spalls with loss of relatively large pieces of tread material Zakharov and Goryacheva (2005), Jérgeus et al. (1999). When the wheel rolls over a flat, it develops high impact forces that may cause further damages to the wheel and rails Vyas and Gupta (2006). Furthermore, above a critical speed, a loss of rail-wheel contact occurs, which produces increased noise and vibrations Wu and Thompson (2002).

Wheel-flats are amongst the most common local surface defects of railway wheels. The repetitive high impact forces involved cause a rapid deterioration of both, rolling and fixed railway structures. The incidence of hot bearings, broken wheels and rail fractures are coincidental with the number of wheel-flats and out-of-round wheels Snyder et al. (2003).

Consequently, there is a great interest in finding methods for an early detection and evaluation of wheel-flats without dismantling the wheelsets due to their complex assembly Pohl et al. (2004). Ideally, to reduce time and costs, the measuring technique should be performed automatically while the train is in motion, even at low speed when it is entering into a maintenance workshop.

Several methods have been put forward to this purpose. Most of them fit into one of the following categories:

(a) *Measurement of the impact forces in an instrumented rail*: the most common system to detect wheel-flats is the Wheel Impact Load Detector (WILD) developed by Salient Systems, Inc. The system consist of a large number of strain gauges mounted in the rail web, which are used to quantify the force applied to the rail through a mathematical relationship

☆ In collaboration with DANO-RAIL, Products and Services for the Railway Maintenance.

* Corresponding author. Tel.: +34 91 871 1900; fax: +34 91 871 7050.
E-mail address: brizuela@iai.csic.es (J. Brizuela).

0968-090X/$ - see front matter © 2011 Elsevier Ltd. All rights reserved.
doi:10.1016/j.trc.2011.04.004

between the applied load and the deflection of the foot of the rail. These impact forces are used to monitor wheels health and to ensure safe train operations Salient Systems (2010), Stratman et al. (2007). In other cases, accelerometers are used instead Belotti et al. (2006). These techniques analyze the impacts produced by flats or other kind of flaws, but give no indications about their size.

(b) *Wheel radius variations measurement*: in this case, the wheel flange is considered perfectly round and wear-free, being used as a reference to estimate the variations in the wheel radius. Mechanical Feng et al. (2000) and optical Gutauskas (1992) systems have been designed based on this idea. Both are sensitive to vibrations, resolution is limited and optical methods are not quite suitable for the railway environment. Furthermore, small irregularities or adherences in the flange will lead to false indications.

(c) *Direct flaw detection and measurement*: ultrasound has been frequently used to detect flaws in the wheel tread. A transducer (EMAT or piezoelectric) is fired when the wheel passes over it, generating a Rayleigh wave that travels around the rolling surface. The same or other transducer receives echoes produced by cracks Ibáñez et al. (2005), Salzburger et al. (2008). Unfortunately, rounded flats are very difficult to detect by this technique, since their smooth edges produce small or no echoes at all.

1.1. Alternative: ultrasonic flat sizing

A different methodology is proposed: an interrogating Rayleigh wave is sent over a measuring rail instead of around the wheel rolling surface. Differently from common ultrasound NDT procedures which are based on the reflectivity of static flaws, this technique analyzes the kinematic of the echo produced by the wheel-rail contact point.

Rayleigh waves are generated by properly adjusting the incidence angle β of the signal emitted by a conventional ultrasound transducer mounted on a plastic wedge. Following the Snell's law, the refracted beam will continue at 0° on the rail (a surface wave) if $\sin(\beta)$ equals the ratio of the propagation velocities in wedge and rail. This way, a short ultrasonic pulse propagates over the measuring rail, eventually producing an echo when it arrives at the wheel-rail contact point Bray et al. (1973).

According to this methodology two alternatives have been studied: in a previous work, velocity changes in the contact point displacement have been detected by Doppler effect, using a monochromatic wave Brizuela et al. (2010b). When the wheel rolls over a perfectly circular part, the contact point velocity is equal to the train speed (assumed constant) and the Doppler frequency shift remains steady. Flats were detected by analyzing the variations of the Doppler frequency shift.

The current work is based on measuring the RTOF of the echo produced by the wheel-rail contact point. As it is shown later, such technique provides a robust method for a quantitative measurement of wheel-flats, independently of their wear state and noise present in the signal. Furthermore, the proposed method provides many other advantages:

- It is a dynamic technique, performing with the train running at low speed (5–10 Km/h typical).
- The invariant set of transducer and measuring rail can be fully characterized, so that results are independent of the particular wheel rolling surface state.
- The measuring device has no moving parts.
- Optimum ultrasound coupling from the transducer to the rail can be achieved.
- It automatically detects the presence of the wheel and measures its speed.
- It has no special environment requirements.

2. Measuring principles

A new wheel-flat is usually modeled as a circumference chord of length L and loss of material d (Fig. 1). At this stage, the wheel-flat edges are singular points, where the curvature changes from the nominal wheel radius R to ∞. By considering the geometry shown in Fig. 1:

$$L = 2\sqrt{2Rd - d^2} \approx \sqrt{8Rd} \tag{1}$$

the original wheel-flat length L can be obtained by measuring d. However, as the wheel continues rolling, the wheel-flat edges become progressively rounded by plastic deformation (partially rounded flat). The wheel-flat part eventually disappears and the profile becomes a continuous curve with a length greater than L, but the depth d remains unchanged (degenerated flat) Baeza et al. (2006). Wheel wear may cause a further increase of the wheel-flat length but, since this process is rather slow and uniform, the loss of material d remains constant until it is removed by a turning machine.

A degenerated wheel-flat can be assumed stable, if it meets the following criteria: (a) the closed region bounded by $r(\theta)$ is convex; (b) $r(\theta)$ is continuous with no singular points, so that $\dot{r}(\theta)$ is also continuous. Otherwise, new plastic deformations will modify the wheel-flat profile until stability is reached, as it happens with new and partially rounded flats. Although not strictly required, it will be also assumed for clearness that the wheel-flat is symmetric around $\theta = 0$, where $r(0) = R - d$.

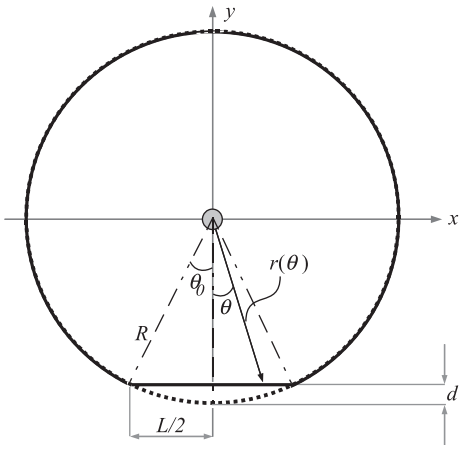

Fig. 1. Geometry of a new wheel-flat (enlarged-scale drawing).

2.1. Theoretical basis

Let us consider a degenerated wheel-flat meeting the stability criteria, defined by the function $r(\theta)$ in the interval $(-\theta_H, \theta_H)$, and $r = R$ for $|\theta| \geqslant \theta_H$ (Fig. 2a). Note that, at $\theta = 0$, the wheel center projection P on the rail coincides with the wheel-rail contact point Q. This situation ($P = Q$) also happens when the wheel rolls over a circular region, since the radius is normal to the tangent at Q. However, when the wheel rolls over an out-of-round region, the vector OQ is not normal to the rail (the rail is always tangent to the wheel at the contact point Q) and, thus, there is a distance s between Q and P.

Denoting by φ the angle rotated by the wheel around its axis O at a given time and by θ the contact point polar coordinate for each φ, when the wheel rotates an angle φ within the interval $(-\theta_H, \theta_H)$: (a) $\theta < \varphi$ and P leads Q for $-\theta_H < \varphi < 0$; (b) $\theta > \varphi$ and Q leads P for $0 < \varphi < \theta_H$. Fig. 2b shows a situation with $\varphi > 0$ (equivalent to the shown rail rotation) where the contact point is ahead the wheel center projection (wheel moves towards $+x$).

The distance $s = PQ$ is given by the scalar product of vector $\vec{OQ} = \vec{r}(\theta)$ and the unity vector $\vec{t}(\theta)$ tangent to the irregularity. This is given by:

$$\vec{t}(\theta) = \frac{\dot{\vec{r}}(\theta)}{\|\dot{\vec{r}}(\theta)\|} \tag{2}$$

$$s(\theta) = \vec{OQ} \cdot \vec{t} = \vec{r}(\theta) \cdot \frac{\dot{\vec{r}}(\theta)}{\|\dot{\vec{r}}(\theta)\|} = \frac{r(\theta)\dot{r}(\theta)}{\sqrt{r(\theta)^2 + \dot{r}(\theta)^2}} \tag{3}$$

As $\dot{r}(\theta) \ll r(\theta)$ in the range $(-\theta_H, \theta_H)$, (3) can be approached by:

$$s(\theta) \approx \dot{r}(\theta) \tag{4}$$

On the other hand, from simple geometry (Fig. 2b):

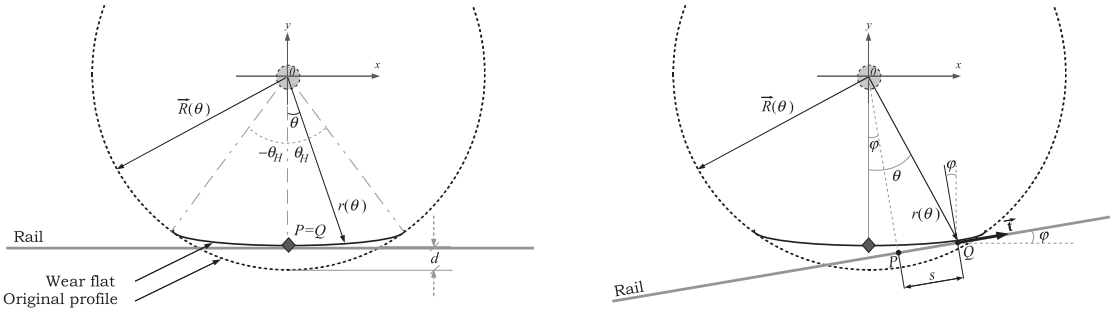

(a) The wheel centre projection P coincides at O with the wheel-rail contact point Q.

(b) The wheel has rotated an angle φ. In this case Q leads P.

Fig. 2. A degenerated wheel-flat in the wheel.

$$s(\theta) = r(\theta)\sin(\theta - \varphi) \tag{5}$$

At the wheel-flat edges, the condition of continuity require $s(\theta_H) = 0$, that is, the projection P coincides with Q since the wheel is rolling over a circular part. As $r(\theta_H) = R$, the rotation angle at the edges must be $\varphi_H = \theta_H$ to satisfy (5).

Since $r(\theta)$ is continuous with decreasing values from $-\theta_H$ to 0 and increasing from 0 to θ_H, its derivative $\dot{r}(\theta)$ will show a negative cycle followed by a positive one as θ changes from $-\theta_H$ to θ_H. Negative values of s indicate that Q lags P and vice versa. Obviously, the positive ones must compensate all the negative deviations, since the wheel is a solid body.

However, in a real application, the function $r(\theta)$ is unknown. But, for the moment, let us assume that there is a method to obtain $s(\varphi)$, that is, the displacement s as a function of the rotated angle φ. The area below $s(\varphi)$ in the range $(0,\varphi_H)$ that represents half the irregularity interval, with $\varphi_H = \theta_H$ is:

$$A = \int_0^{\varphi_H} s(\varphi)\ \mathrm{d}\varphi = \int_0^{\theta_H} s(\theta)\ \mathrm{d}\theta \approx \int_0^{\theta_H} \dot{r}(\theta)\ \mathrm{d}\theta = r(\theta_H) - r(0) \tag{6}$$

By definition $r(\theta_H) = R$ and $r(0) = R - d$. Therefore,

$$d = \int_0^{\varphi_H} s(\varphi)\ \mathrm{d}\varphi \tag{7}$$

gives the loss of material by abrasion d as a function of the measured displacement $s(\varphi)$. On the other hand, as $s(\varphi)$ is a continuous function even if singular points are present, the result (7) is valid for any kind of wheel-flats (new, partially rounded or degenerated with any degree of wear). The same result is obtained for $-s(\varphi)$ if the integral is extended to the interval $(-\varphi_H, 0)$. This leads to the following property:

For small irregularities, the area below $|s(\varphi)|$ *approximates two times the loss of material* d.

As a result, whatever is the wheel-flat wear from the original one, (7) gives the loss of material d. Also, since $s(\varphi) = 0$ in the round part of the wheel ($|\varphi| > \varphi_H$), for single or isolated flats the integral may be extended to any angle $\varphi_A \geqslant \varphi_H$. By incorporating a parameter α to cover a full wheel revolution, $0 \leqslant \alpha \leqslant 2\pi - \varphi_A$, (7) can be written as follows:

$$d(\alpha) = \int_{\alpha}^{\alpha+\varphi_A} s(\varphi)\ \mathrm{d}\varphi, \quad 0 \leqslant \alpha \leqslant 2\pi - \varphi_A \tag{8}$$

This formulation allows the evaluation of d as a function of α for a whole wheel revolution, as long as $\varphi_A \geqslant \varphi_H$.

3. Measurement

Fig. 3 shows the arrangement to measuring $s(\varphi)$. A transducer, located at one end of the rail, generates ultrasound pulses of Rayleigh waves with a period T_{PRF}. The pulses travel on the rail surface and reach the wheel contact point Q, which produces an echo. The rail-wheel contact position obtained from measuring the RTOF ($T_{Q(i)}$) of a pulse i is:

$$x_{Q(i)} = \frac{c\ T_{Q(i)}}{2} \tag{9}$$

where c is the propagation velocity for Rayleigh waves.

Assuming that the train moves at a constant speed v, the wheel center projection after i pulses is:

$$x_{P(i)} = i\ T_{PRF}\ v \tag{10}$$

Then, the distance $s(i) = x_{Q(i)} - x_{P(i)}$ is:

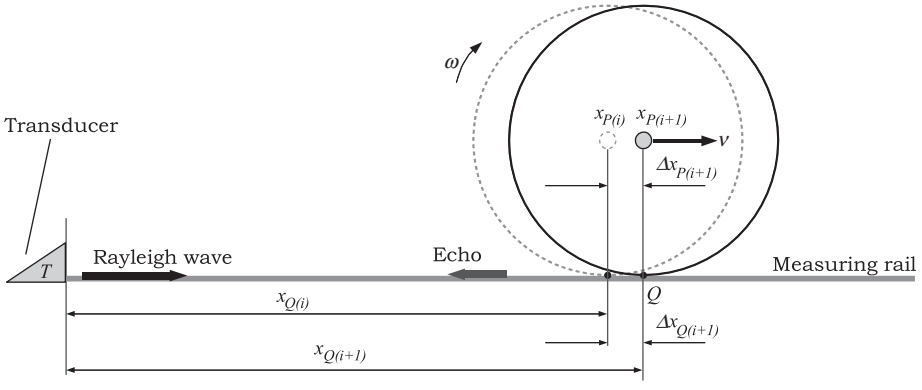

Fig. 3. Measuring arrangement.

$$s(i) = \frac{c\ T_{Q(i)}}{2} - i\ T_{PRF}\ v \tag{11}$$

For a sampled system, the integral in (8) can be replaced by:

$$d \approx \sum_i s(i)\ \Delta\varphi \tag{12}$$

$$\Delta\varphi = \omega\ \Delta t = \frac{v\ T_{PRF}}{R} \tag{13}$$

The sum (12) is extended over M samples of $s(i)$, where M should be chosen to cover at least half the largest irregularity. Since the sampling period of $s(i)$ is T_{PRF} and, if L_{max} is the length of the largest flat of interest,

$$M \geqslant \frac{L_{max}}{2\ v\ T_{PRF}} \tag{14}$$

Following the pulse k,

$$d_k^M = \frac{v\ T_{PRF}}{R} \sum_{i=k}^{k+M} s(i) \tag{15}$$

where $s(i)$ is given by (11) and M is the discrete version of the angle φ_A in (8). The measuring process is carried out as a convolution of a rectangular unity window of M samples with the values of $s(i)$. The sequence $\{d_k^M\}$ represents the value of the loss of material d, which is estimated following pulse k with a window of size M. Since the window must be wider than the flaw, the peak value of this sequence corresponds to the best estimation of d for isolated wheel-flats.

3.1. Train speed and loss of material estimation

The same measuring system provides a very simple method to obtain the value of v required by (15). The position of the contact point Q following the pulse $i + 1$ is,

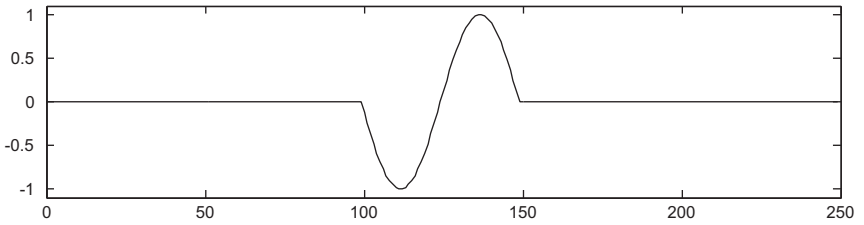

(a) Displacement signal s.

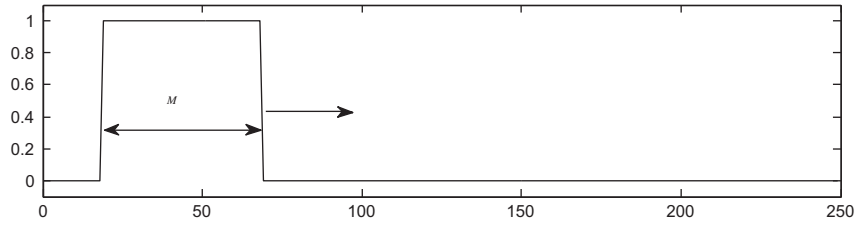

(b) Rectangular unity window $\mathbf{w}$.

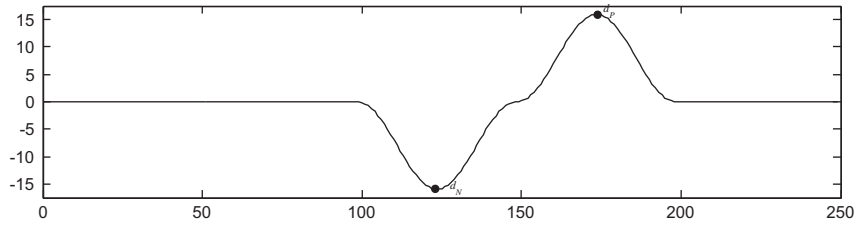

(c) Sequence $\{d_k\} = s * \mathbf{w}$.

Fig. 4. Sequence $\{d_k(M)\}$ obtained as the convolution of s with a unit window of length M.

$$x_{Q(i+1)} = x_{Q(i)} + T_{PRF}\ v_{Q(i)} \tag{16}$$

The RTOF $T_{Q(i+1)}$ is:

$$T_{Q(i+1)} = \frac{2\ x_{Q(i+1)}}{c} = T_{Q(i)} + \frac{2 v_{Q(i)}}{c} T_{PRF} \tag{17}$$

$$v_{Q(i)} = \frac{T_{Q(i+1)} - T_{Q(i)}}{2\ T_{PRF}}\ c = \frac{\Delta T_{Q(i)}}{2\ T_{PRF}}\ c \tag{18}$$

where (18) gives the instantaneous velocity of the contact point Q following the pulse i and all the parameters are known or measured. As any loss in velocity of Q must be compensated by a subsequent increment, taking the average of N measurements gives an estimation of the train mean speed v:

$$v = \hat{v}(j) = \frac{1}{N} \sum_{i=j}^{i=j+N-1} v_{Q(i)} \tag{19}$$

Fig. 4 shows graphically the process. For a given value of M samples, the resulting sequence $\{d_k\}$ has two peaks, one negative d_N and another positive, d_P, which correspond to the negative and positive cycles of s. If it is scaled by the factor vT_{PRF}/R, their absolute value should be equal to d. In real applications, where noise is present, d is approached by the peak-to-peak average:

$$d_E(M) = \frac{vT_{PRF}}{R} \frac{d_P(M) + d_N(M)}{2} \tag{20}$$

From the estimated value d_E, the equivalent length of the original wheel-flat L_E can be obtained by application of (1).

This process requires also the knowledge of the wheel radius R, whose value may be smaller than the nominal one due to the wheel wear. However the relative error is low, since wheels are not kept in service if the radius has decreased by more of a small percentage from the nominal one (10% typical).

On the other hand, the approximation of the integral by a sum produces biased d_E values. To take these effects into account, a correction may be done by multiplying the resulting d_E value by a constant γ, typically in the range $1 < \gamma < 1.2$.

4. Performance of the technique with noisy measurements

The RTOF $T_{Q(i)}$ is required to compute $s(i)$ and $v_{Q(i)}$ (Eqs. (11) and (18)). This may be simply evaluated by looking at the position of the absolute signal value maximum in a gate that includes the echo position. To this purpose, an algorithm that tracks the contact-point echo displacement has been hardware implemented Brizuela et al. (2010a). However, electrical and grain noise contaminate the signals, leading to variations in the measured position.

Nevertheless, the method is very robust with noisy signals, due to the integration performed by (15). Fig. 5a shows the simulated sequence $\{s(i)\}$ for a degenerated wheel-flat with $d = 0.4$ mm in a wheel of $R = 500$ mm. It has been acquired at intervals $\Delta x = vT_{PRF} = 0.6$ mm in a rail with $c = 3000$ m/s. This sequence has been deeply contaminated with white Gaussian noise to represent a considerable uncertainty in finding the actual echo position after every pulse i due to noise.

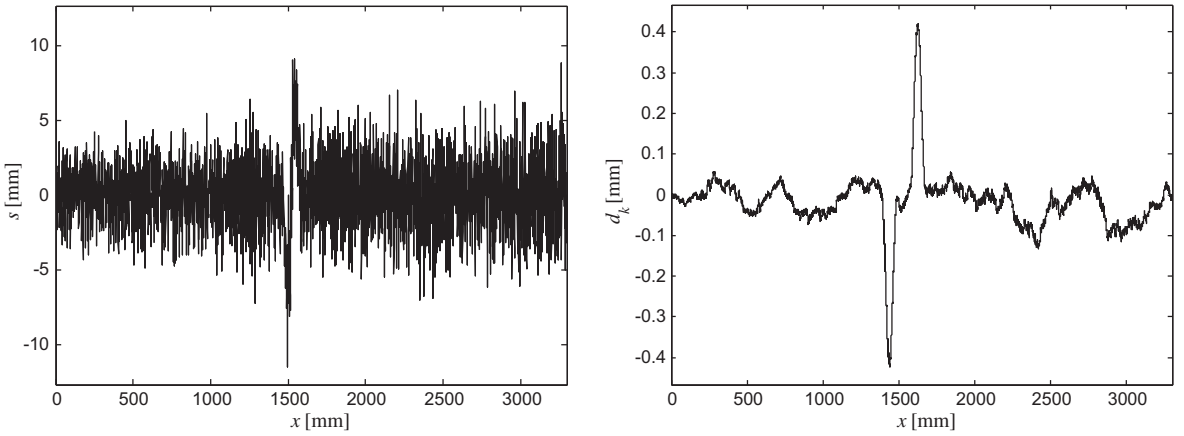

(a) Sequence {s(i)} deeply contaminated with white gaussian noise.

(b) Resultant $\{d_k\}$ sequence.

Fig. 5. Simulation parameters: $R = 500$ mm, $c = 3000$ m/s, $d = 0.4$ mm, $vT_{PRF} = 0.6$ mm.

Fig. 5b shows the sequence $\{d_k\}$ obtained from the noisy $\{s(i)\}$ by application of (15) with a window of $M = 267$ samples. Following (14), this corresponds to a maximum wheel-flat length of $L_{max} = 320$ mm. It can be seen the filtering effect of the sum, as well as the agreement of the negative and positive peaks with the correct $d = 0.4$ mm value ($d_N = 0.4275$ mm, $d_P = 0.4383$ mm). The averaged estimation is $d_E = 0.43$ mm.

5. Experimental results

To validate the performance of the proposed technique an experimental test bench has been arranged (Fig. 6a). A 1 MHz piezoelectric transducer generates Rayleigh wave pulses in a 2000 mm long measuring rail. A pair of wheel treads with $R = 420$ mm were used to perform the experimental work. An UltraSCOPE®, Dasel Sistemas (2010), ultrasonic testing system was modified to include the tracking algorithm. The recorded echo signals were sent through a USB 2.0 interface to an evaluation computer. The transducer was excited with a pulse repetition period T_{PRF} of 2 ms. The gain was varied by a Time-Gain-Compensation (TGC) function adapted to receive similar contact-point echo amplitudes from different distances.

Grain noise and many propagation modes in the measuring rail contaminated the signal. That noise was partially removed because it is mostly static. Electrical noise was also reduced by applying a narrow-bandpass 63-coefficients FIR filter, also available in the UltraSCOPE® system.

Artificial wheel-flats were mechanized over the tread wheels. Fig. 6b and c show the test profiles measured with a mechanical comparator. The maximum material loss for the *wheel-flat* #1 is $d = 0.46$ mm. By application of (1) this corresponds to a new wheel-flat length of $L = 39.3$ mm. A simple comparative between measured and new profiles can be also done in Fig. 6b. Note that the *wheel-flat* #1 profile corresponds to an asymmetric partially rounded flat.

Taking into account the *wheel-flat #2* profile shown in Fig. 6c, in this case, its shape is slightly concave (a cavity). This artificial flaw emulates a new wheel-flat, since it is not possible to roll over a cavity. The corresponding new wheel-flat is defined by $d = 0.20$ mm which yields to a length of $L = 25.9$ mm.

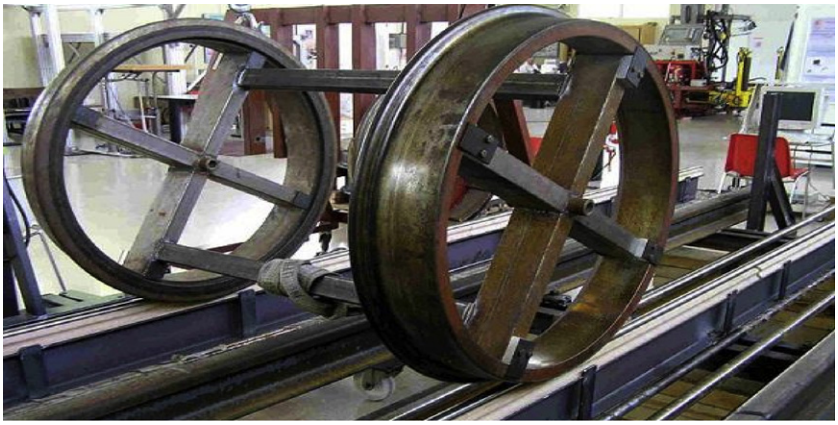

(a) Experimental test bench.

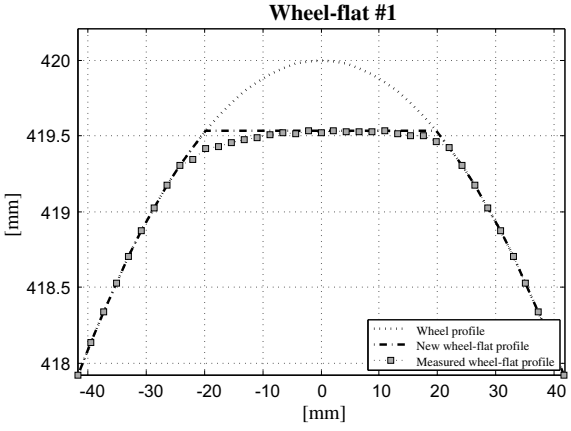

(b) Artificial wheel-flat profile mechanized on wheel #1.

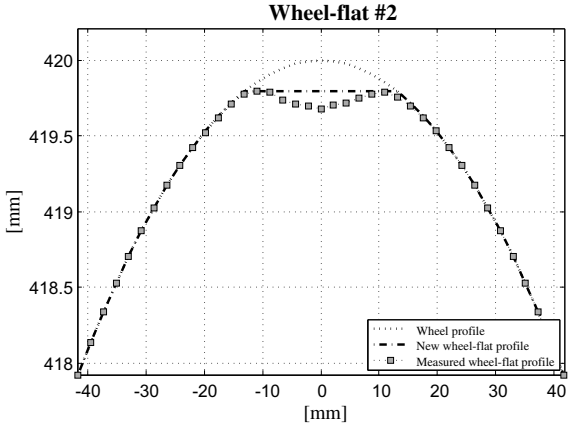

(c) Artificial wheel-flat profile mechanized on wheel #2.

Fig. 6. Prototype inspection system.

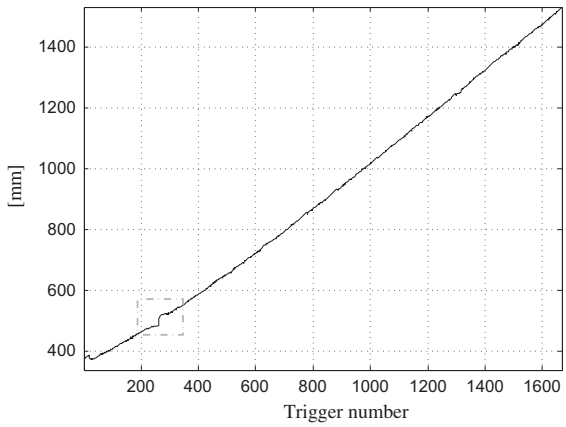

(a) Rail-wheel contact position $x_{Q(i)}$.

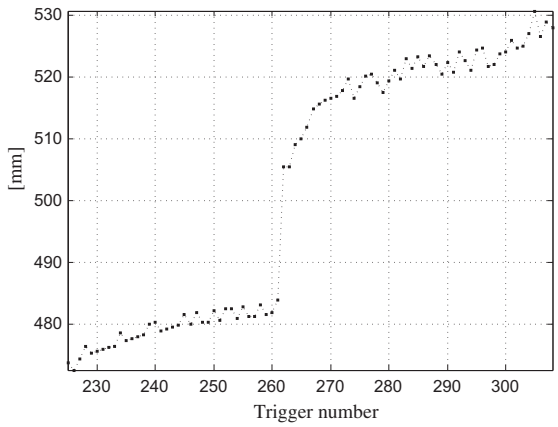

(b) Detailed view of (a).

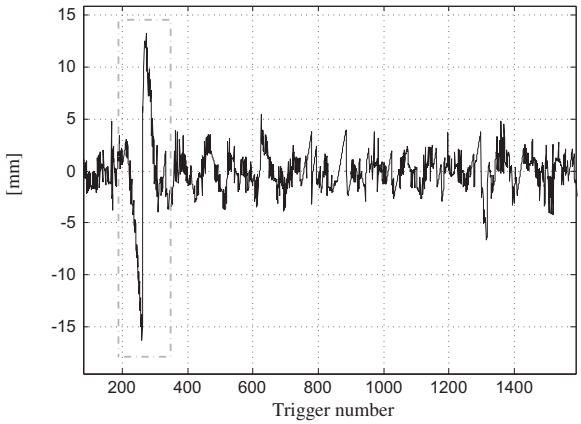

(c) Displacement s as a function of the trigger number.

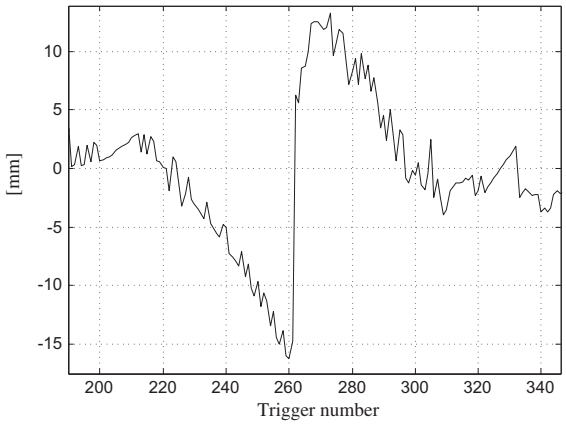

(d) Detailed view of (c).

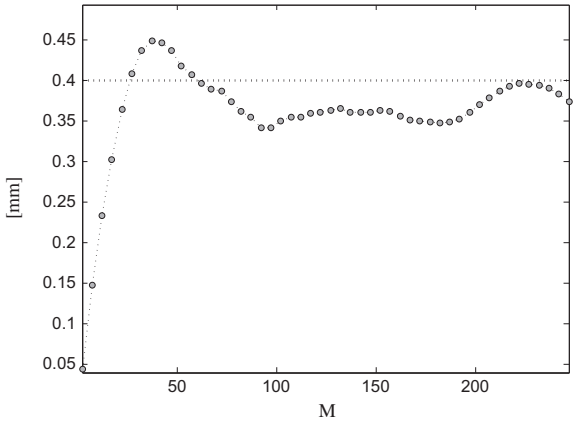

(e) Estimated loss of material as a function of the window length $d_E(M)$.

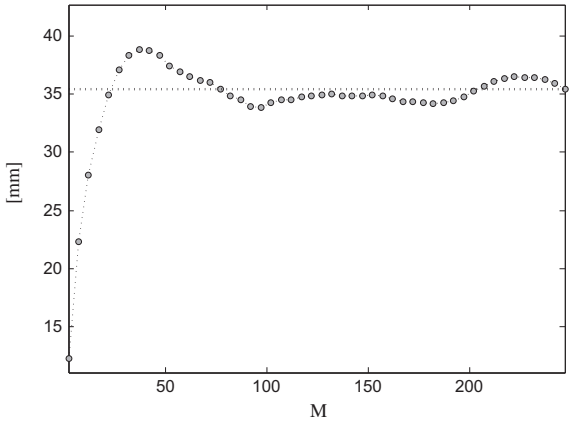

(f) Estimated length as a function of the window length $L_E(M)$.

Fig. 7. Experimental results. (a) Wheel position obtained by measuring the RTOF ($T_{Q(i)}$). (b) RTOF around the flat as a function of the trigger number. Mean speed near the flat region $v \approx 0.33$ m/s and the sampling interval in spatial coordinates $\Delta x = 0.66$ mm. (d) Displacement s around the flat region. (e) Estimated loss of material $d_E(M)$: $d_{E_{max}} = 0.45$ mm, $d_{E_{mean}} = 0.40$ mm, $\sigma_{d_E} = 0.03$ mm. (f) Estimated new flat length $L_E(M)$: $L_{E_{max}} = 38.90$ mm, $L_{E_{mean}} = 35.40$ mm and $\sigma_{L_E} = 1.25$ mm.

5.1. Evaluation process

The wheelset was moved by hand over the measuring rail each time the inspection process has been performed, so that the speed was not quite constant. However, the rail-wheel contact position $x_{Q(i)}$ is obtained by (9) as a function of the

Table 1
Wheel-flats evaluation.

Parameter		Wheel-flat#1			Wheel-flat#2		
Loss of material	d (mm)		0.46			0.20	
Equivalent new wheel-flat length	L (mm)		39.3			25.9	
Distance to transducer	x (mm)	500	1000	2000	700	900	1300
Mean speed	v (m/s)	0.33	0.45	0.54	0.21	0.25	0.34
Sampling interval	Δ_x (mm)	0.66	0.90	1.62	0.42	0.50	0.68
Highest estimation	$d_{E_{max}}$ (mm)	0.45	0.48	0.56	0.21	0.20	0.16
Estimated maximum length	$L_{E_{max}}$ (mm)	38.90	40.75	43.72	27.07	26.16	23.57
Relative error	$\varepsilon(L_{E_{max}})$ (%)	−1.01	3.68	11.32	4.51	0.10	−8.99
Estimated average length	$L_{E_{mean}}$ (mm)	35.40	36.03	40.30	24.14	23.02	21.06

Defects have been located at different distances from the transducer.

Table 2
New wheel-flat estimated at different wheel speed.

Parameter		Wheel-flat #1									
Decimation factor	n	1	2	3	4	5	6	7	8	9	10
Mean speed	v (m/s)	0.33	0.62	0.94	1.25	1.56	1.87	2.18	2.49	2.80	3.28
Spatial sampling interval	Δx (mm)	0.66	1.31	1.97	2.62	3.28	3.94	4.60	5.25	5.90	6.56
Window size	M (samples)	38	20	12	12	9	7	7	6	5	5
Estimated maximum length	$L_{E_{max}}$ (mm)	38.90	39.10	38.29	40.01	40.45	39.24	37.75	39.06	37.74	40.14
Relative error	$\varepsilon(L_{E_{max}})$ (%)	−1.01	−0.50	−2.57	1.80	2.92	−0.15	−3.94	−0.61	−3.97	2.14
Estimated average length	$L_{E_{mean}}$ (mm)	35.40	36.22	34.32	36.90	36.43	35.88	34.28	33.12	33.09	32.80

The recorded signal shown on Fig. 7c has been decimated to increase the wheel speed.

measured RTOF $T_{Q(i)}$ and the propagation velocity $c = 2970$ m/s. Consequently, the mean speed v can be also estimated for every position in the rail by application of (19).

The *wheel-flat #1* was tried out under this procedure. The estimated mean speed near the flat region was $v \approx 0.33$ m/s and the spatial sampling interval was $\Delta x = vT_{PRF} = 0.66$ mm. Fig. 7a shows the contact point distance $x_{Q(i)}$ as a function of the trigger number. Note the jump in x_Q when the wheel rolled over the wheel-flat, shown with more detail in Fig. 7b. The current wheel-flat length can be obtained from this graph by observing the slope of x_Q which changes between triggers #230 and #290, that is, an interval $\Delta t = 120$ ms at $T_{PRF} = 2$ ms. The wheel-flat length can be easily found out by multiplying the train speed v and Δt, which yields to $L = 39.6$ mm. Nevertheless, this method of performing the measurement is rather imprecise, since it depends on finding the points where x_Q changes the slope. Moreover, it gives no information about the dimensions of the original new wheel-flat (length and loss of material). Therefore, it is much better to estimate the original loss of material d by the process indicated before.

Fig. 7c shows the displacement s around the flat region computed by application of (11). This sequence is contaminated by the uncertainty of locating the exact position of the echo signal due to residual noise. Then, (15) was applied with different window widths ($2 \leqslant M \leqslant 250$), obtaining $d_E(M)$ from (20).

Fig. 7e shows the resulting estimation of d_E as a function of M. It can be seen that, for M values below those indicated by (14), that is, $M < 20$, the estimated d_E value shows errors. Above this figure, the estimation remains near the true value (0.46 mm), with an average $d_{E_{mean}} = 0.40$ mm and a standard deviation $\sigma_{d_E} = 0.03$ mm, in agreement with theory. In fact, this advises of using a large value for M, because this has little impact in the measurement of isolated wheel-flats. The maximum M value should be chosen to avoid including multiple flats into a single window.

Fig. 7f shows the corresponding $L_E(M)$ values, using the estimations $d_E(M)$ and (1). The average value $L_{E_{mean}}$ is 35.4 mm with a standard deviation $\sigma_{L_E} = 1.25$ mm. Note that the equivalent new wheel-flat length is 39.3 mm. These results show a small error by defect, which are due to the approximation of the integral (8) by the sum (15).

Following this methodology, both artificial wheel-flats were evaluated in several positions over the measuring rail in order to put them under different conditions of structural noise interference. On Table 1 the obtained results of these experiments have been summarized. Note that as the wheel speed has not been controlled, the spatial sampling interval is different for each test.

For all cases, the lower relative error with regard to the true value is reached when the integration window extent is close to the defect length, so the estimation is maximum. However, the error increases when measurements are made beyond 1300 mm of the transducer, where the interrogation pulse attenuation is important and the structural noise interference on the echo signal is higher, increasing the error on the contact point position. Nevertheless, the estimated lengths corresponding to the *wheel-flat #1* have been obtained with a relative error below 12%.

On the other hand, detecting the *wheel-flat #2* is more difficult because it is smaller. In this case, the amplitude of the displacement signal s is comparable to the residual noise. However, the lengths have been estimated with an error below 9%, which confirms experimentally the robustness of the method.

The performance of this technique has been also tested by making the measurements at multiple speeds (up to 3 m/s). The recorded displacement signals were decimated in order to increase the wheel speed. Table 2 contains the wheel-flat length estimations corresponding to the displacement signal shown in Fig. 7c. In this case, the integration window size was bounded to M_x = 150 mm. The maximum length estimated is obtained when the window size is close to the equivalent new wheel-flat length (39.9 mm), however fewer samples are contained on M as the speed increases.

The estimated maximum lengths of the new wheel-flat at different speeds remain close to the true value with relative errors that do not exceed 4%, which means an inaccuracy of 1.6 mm. Observe that, if the train speed increases, the spatial sampling interval will increase as well. Consequently, the average wheel-flat lengths tend to decrease and the system resolution will be also reduced.

6. Conclusion

An innovative technique to detect and measure wheel-flats in the rolling surface of railway wheels has been disclosed. It uses Rayleigh wave ultrasonic pulses sent at regular intervals over a measuring rail. The RTOF measurement to the wheel-rail contact point is analyzed. The wheel-flats are quantified by the sum of the displacements of the wheel-rail contact point to the wheel center projection on the rail, which yields the loss of material produced by abrasion in the original wheel-flat. These displacements are obtained from the measured RTOF and the wheel displacement velocity, which is also estimated by the proposed technique.

The technique performance has been tested by simulation using noisy signals and wheel-flats with different stage of roundness. Results have shown that the method is robust against noise and the measurement is independent of the wheel wear degree and the wheel-flat roundness.

In addition, two artificial wheel-flats of 40 and 26 mm length with different wear degree have been used to demonstrate the technique by experimentation. The wheel-flats have been evaluated in different positions over the measuring rail and the estimated lengths remain close to the true value in both cases with a low relative error.

The inspection speed has also been taken into account. The stored displacement signals have been decimated in order to increase the wheel speed. As a result, the system resolution decreases as the speed increases, nevertheless the estimated lengths kept near the real value with relative errors below 4% at maximum speed (3 m/s).

The lower the circulation speed, the greater the resolution of the technique. Finally, it has also many other advantages for the railway industry, as being a dynamic technique, without moving parts and a well characterized and stable measuring arrangement. The method allows all the wheelsets mounted in a train to be inspected within a few seconds.

References

Baeza, L., Roda, A., Carballeira, J., Giner, E., 2006. Railway train-track dynamics for wheelflats with improved contact models. Nonlinear Dynamics 45, 385–397.

Belotti, V., Crenna, F., Michelini, R., Rossi, G., 2006. Wheel-flat diagnostic tool via wavelet transform. Mechanical Systems and Signal Processing 20 (8), 1953–1966.

Bray, D., Dalvi, N., Finch, R., 1973. Ultrasonic flaw detection in model railway wheels. Ultrasonics 11 (2), 66–72.

Brizuela, J., Ibáñez, A., Fritsch, C., 2010a. NDE system for railway wheel inspection in a standard FPGA. Journal of Systems Architecture 56, 616–622.

Brizuela, J., Ibáñez, A., Nevado, P., Fritsch, C., 2010b. Flaw detector for railways wheels by doppler effect. Physics Proceedia 3 (1), 811–817.

Dasel Sistemas, 2010. Ultrasound technology. <http://www.daselsistemas.com> (viewed 07.05.11).

Feng, Q., Cui, J., Zhao, Y., Pi, Y., Teng, Y. 2000. A dynamic and quantitative method for measuring wheel flats and abrasion of trains. In: 15th World Congress on NDT, Rome, Italy.

Gutauskas, P., 1992. Railroad flat wheel detectors. US Patent No. 5 133 521.

Ibáñez, A., Parrilla, M., Fritsch, C., Giacchetta, R., 2–4 November, 2005. Inspecci=n mediante ultrasonidos de ruedas de tren en operaciones de mantenimiento. In: V CORENDE, Neuquén, Argentina.

Jérgeus, J., Odenmark, C., Lundén, R., Sotkovszki, P., Karlsson, B., Gullers, P., 1999. Full-scale railway wheel flat experiments. Proceedings of the Institution of Mechanical Engineers, Part F 213, 1–13.

Pohl, R., Erhard, A., Montag, H.-J., Thomas, H.-M., Wüstenberg, H., 2004. NDT techniques for railroad wheel and gauge corner inspection. NDT&E International 37, 89–94.

Salient Systems, Inc., 2010. Intelligent track solutions. <http://www.salientsystems.com> (viewed 07.05.11).

Salzburger, H.J., Wang, L., Gao, X., 25–28 October, 2008. In-motion ultrasonic testing of the tread of high-speed railway wheels using the inspection system AUROPA III. In: 17th World Conference on NDT, Shangai, China.

Snyder, T., Stone, D.H., 22–24 April, 2003. Wheel flat and out-of-round formation and growth. In: Proc. 2003 IEEE/ASME Joint Rail Conf., Chicago, Illinois, pp. 143–148.

Stratman, B., Liu, Y., Mahadevan, S., 2007. Structural health monitoring of rail road wheels using impact load detectors. Journal of Failure Analysis and Prevention 7 (3), 218–225.

Vyas, N.S., Gupta, A.K., 2006. Modeling rail wheel-flat dynamics. In: Engineering Asset Management. Springer, London, pp. 1222–1231.

Wu, T.X., Thompson, D.J., 2002. A hybrid model for the noise generation due to railway wheel flats. Journal of Sound and Vibration 251 (1), 115–139.

Zakharov, S.M., Goryacheva, I.G., 2005. Rolling contact fatigue defects in freight car wheels. Wear 258, 1142–1147.